AIAA'83

AIAA-83-2093

Optimization and Closed-Loop Guidance of Drag-Modulated Aeroassisted Orbital Transfer

J.A. Kechichian, M.I. Cruz and E.A. Rinderle,
Jet Propulsion Lab., Pasadena, CA; and N.X.
Vinh, Univ. of Michigan, Ann Arbor, MI

AIAA Atmospheric Flight Mechanics Conference

August 15-17, 1983/Gatlinburg, Tennessee

OPTIMIZATION AND CLOSED LOOP GUIDANCE
OF
DRAG MODULATED
AEROASSISTED ORBITAL TRANSFER

J. A. Kechichian*, M. I. Cruz**, N. X. Vinh+,
E. A. Rinderle***

Abstract

An analysis of optimal and near optimal atmospheric flight trajectories for drag modulated aeroassisted orbital transfer is presented. An explicit and adaptive closed loop guidance approach for this mode of orbit transfer is also presented with performance near the optimal nominal trajectories. The orbital transfer of interest is for return from high Earth orbit to low Earth orbit. Most of what is discussed in this paper concerns the aeroassisted or atmospheric segment which lowers the apogee of the high Earth orbit to the apogee of the low Earth orbit. *Minimization of the total impulsive* ΔV *at* this low Earth orbit apogee is the optimization criterion. Control about this impulse due to a number of potential error sources in atmospheric braking is the requirement imposed on closed loop guidance.

Introduction

Two concurrent studies were performed to research drag modulated entry of Aeroassisted Orbital Transfer Vehicles (AOTV)[1,2]. These consisted of analyses which dealt with formulation of the optimal control problem,[3] and formulation of closed loop guidance strategies and mechanizations which minimize the effect of external variables and arrive at near optimal orbital transfer.[4] It is desired that the closed loop guidance be absolutely explicit and adaptive. This paper discusses the analytical development and engineering analyses of these studies.

In the first part of this paper, the analysis of the optimal flight path control of a purely drag modulated orbit transfer vehicle is presented. The strategy consists of eliminating *the circularizing* ΔV *of the Hohmann transfer* by applying a slightly higher deorbit ΔV such that the conic perigee of the elliptic transfer orbit is located inside Earth's atmosphere where the required velocity depletion is obtained through aerobraking. Flight path control must then be carried out during the atmospheric portion of the *flight in order to exit from the atmosphere with* the appropriate velocity V_f and flight path angle γ_f that transfers the vehicle to the desired low circular orbit on an elliptic transfer orbit tangent to it at its apoapse.

A small circularizing ΔV_2 is finally needed *at the tangency point to enter the final orbit.* It is shown that there exists an optimal pair (V_f, γ_f) that results in minimum ΔV_2 among the infinitely many such pairs. The optimal control problem is cast into its most general form and the overall minimum ΔV transfer analyzed by considering initial and final side constraints. The appropriate *transversality conditions at entry* and exit corresponding to initial and final times, are then developed and a backward numerical integration scheme devised that integrates both state and adjoint equations using the optimal scalar control variable C_D that maximizes the variational Hamiltonian. It is shown that the *control is of the bang-bang type, switching* C_D between its $C_{D_{min}}$ and $C_{D_{max}}$ upper and lower bounds with no intermediate level control possible, C_D appearing linearly in the Hamiltonian.

The closed loop guidance strategies and mechanization presented suggest truly adaptive and *explicit performance. They provide near optimal* trajectory performance with significant trajectory accuracy control capability.

The mode of drag modulation is of no interest to this study. That is, this analysis assumes that a capability will exist to provide ballistic *coefficient* ($\beta = m/C_D A$) *control within a required* range of $C_{D_{max}}$-to-$C_{D_{min}}$. This capability can be either from a forward firing engine, a diffuser or any other type of variable geometry device. The requirement as to the $C_{D_{max}}$-to-$C_{D_{min}}$ ratio can be determined from this analysis. This is in the range of 10:1 to 25:1 depending on navigation capability and time allowed to effect the orbital transfer. An additional requirement that needs to be imposed is that at no instant should the entry vehicle develop lift.

Discussion

Optimal Orbital Transfer

The *optimal transfer between coplanar* circular orbits is a Hohmann transfer using two ΔV's applied 180° apart if the High Earth Orbit (HEO) radius, r_1, is less than 11.938765 times the Low Earth Orbit (LEO) radius, r_2, or $r_1 < 11.938765\ r_2$. A biparabolic transfer is optimal for $r_2 > 11.938765\ r_1$. In order to minimize ΔV *further, aeroassisted transfer modes can be* considered to eliminate the second chemical burn by targeting the orbit transfer vehicle to a perigee located inside the atmosphere in order to achieve the required velocity depletion through

* Member of Technical Staff, Navigation Systems Section, JPL
Member AIAA

** Supporting Research and Technology Manager, Systems Division,
JPL, Member AIAA

+ Professor of Aerospace Engineering, University of Michigan

*** Senior Computing Analyst, Mission Design Section, JPL

aerobraking. A small circularizing ΔV_2 is needed later to transfer the vehicle to LEO. This is reflected in Figure 1.

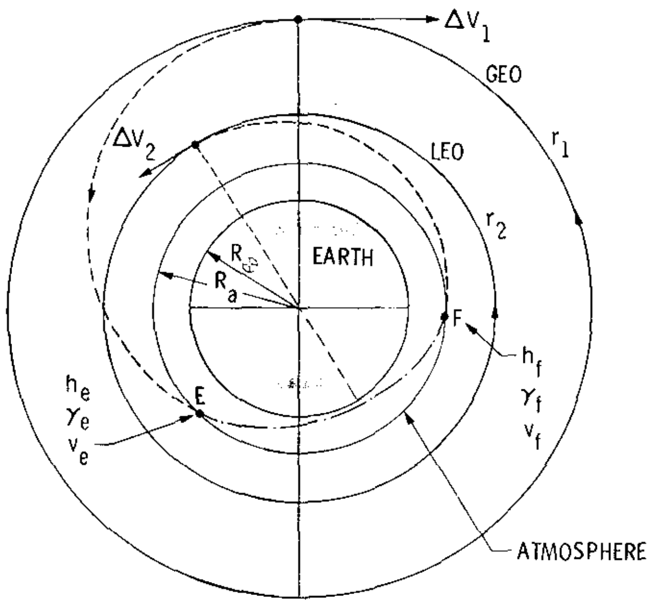

Figure 1

A comparison can be made to determine whether Hohmann, biparabolic or aeroassisted transfers are optimal. This assumes that the optimal aeroassisted transfer can be bounded by a grazing trajectory of the atmosphere. Let

$$\alpha_1 = \frac{r_1}{R_a} \quad , \quad \alpha_2 = \frac{r_2}{R_a} \quad , \quad \Delta v_i = \frac{\Delta V_i}{\sqrt{\mu/R_a}} \qquad (1)$$

The elliptic grazing trajectory requires an impulse of

$$\Delta v_1 = \sqrt{\frac{1}{\alpha_1}} - \sqrt{\frac{2}{\alpha_1(\alpha_1+1)}} \qquad (2)$$

while the parabolic grazing trajectory requires theoretically two impulses

$$\Delta v_1 + 0 = \sqrt{\frac{2}{\alpha_1}} - \sqrt{\frac{1}{\alpha_1}} \qquad (3)$$

In this mode, the first impulse is used to send the vehicle into a parabolic orbit from HEO and the second infinitesimal impulse at infinity (in practice at a large distance from Earth) to graze the atmosphere.

In order to obtain the total characteristic velocity for the aeroassisted mode, the circularizing ΔV_2 at r_2 must be added to the above ΔV's. This is found to be

$$\Delta v_2 = \sqrt{\frac{1}{\alpha_2}} - \sqrt{\frac{2}{\alpha_2(\alpha_2+1)}} \qquad (4)$$

These sums must be compared with the all propulsive Hohmann and biparabolic transfers which are found to be, respectively, as follows

$$\Delta v_H = \sqrt{\frac{1}{\alpha_1}} - \sqrt{\frac{2\alpha_2}{\alpha_1(\alpha_1+\alpha_2)}} + \sqrt{\frac{2\alpha_1}{\alpha_2(\alpha_1+\alpha_2)}} - \sqrt{\frac{1}{\alpha_2}} \qquad (5)$$

$$\Delta v_P = \frac{(\sqrt{2}-1)}{\sqrt{\alpha_1}} + \frac{(\sqrt{2}-1)}{\sqrt{\alpha_2}} \qquad (6)$$

to determine the absolute optimal transfers.

In summary, we have the following transfer modes:

- A_1: aeroassisted transfer with grazing elliptic orbit
- A_2: aeroassisted transfer with grazing parabolic orbit
- B_1: Hohmann transfer
- B_2: biparabolic transfer

For given values of α_1 and α_2, the orbital transfer mode can be determined. For elliptic and parabolic transfers, the following explicit criteria can be made

Mode A_1 is better than mode A_2 if $\alpha_1 < 4.828427$
Mode B_1 is better than mode B_2 if $\alpha_1 < 11.938765\alpha_2$ (7)

The comparison between mode A and B is by direct verification. In particular, mode A_2 is better than mode B_2 if $\alpha_2 < 4.828427$. The comparison between mode A_1 and B_1 is shown in Figure 2. Of special interest should be the return from Geosynchronous Earth Orbit (GEO) to LEO where $\alpha_1 = 6.50062$ and $\alpha_2 = 1.0354$. The aeroassisted orbital transfer is absolutely superior to the all propulsive orbital transfer.

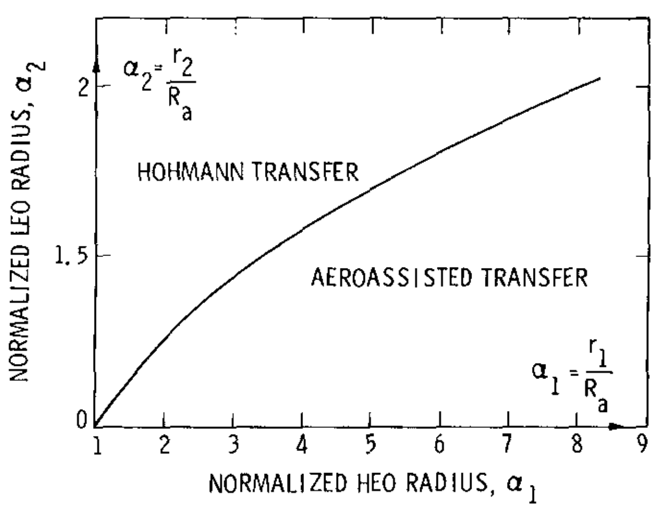

Figure 2

An additional element that must be considered in this analysis is plane change when comparing elliptic and biparabolic drag modulated aeroassisted orbital tansfer. The biparabolic can have additional savings, since the ΔV associated with plane change at infinity is very small.

Aeroassisted Orbital Transfer Optimization Approach

It has already been determined in Reference 1 that a split-ΔV strategy be adopted for the ΔV_1 burn. This is due to the large magnitude of this burn (greater than 2 km/sec), since direct-entry after this burn could potentially result in entry flight path angle errors on the order of $\pm 5^o$. Therefore, the first part of ΔV_1 will place the entry vehicle barely outside the atmosphere and return to its HEO apogee. A small ΔV is then applied at apogee to lower perigee inside the atmosphere with acceptable accuracy.

A preliminary analysis indicates that almost all of the savings in ΔV take place at the circularizing burn and that the atmospheric flight path is shaped in order to exit with a state vector that corresponds to the highest energy possible elliptic transfer orbit to LEO. Figure 3 shows a plot of the exit conditions which will result in a 200 km LEO. It also shows the ΔV_2 associated with each exit condition. It demonstrates that minimizing γ_f will result in a minimum ΔV_2 solution. In fact, if the absolute minimum γ_f of zero could be obtained, the ΔV_2 would be as small as 18 m/sec.

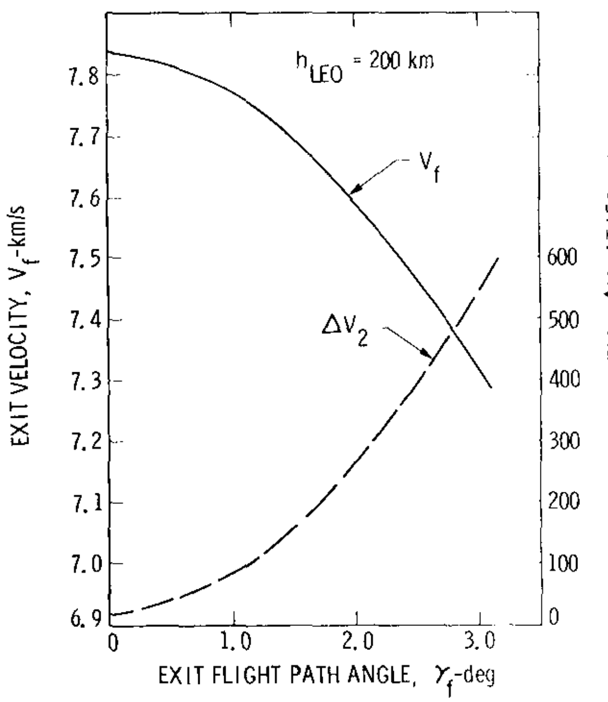

Figure 3

Here, the atmospheric flight model assumed a spherical and non-rotating Earth which is adequate for a first order solution to the coplanar orbital transfer problem. The iteration scheme shown in Appendices 1 and 2 require an adequate guess of the exit flight path angle in order to converge rapidly on the optimal solution. In order to gain more insight into this drag modulated problem and provide the optimization scheme with the appropriate initial starting guess for a given orbit transfer from a HEO to a LEO, a series of near optimal trajectories are generated by considering only one switch from C_{Dmax} to C_{Dmin} at varying switch times τ_s for different conic perigee targets or entry states. The system equations (1-9) - (1-11) of Appendix 1 are integrated forward from entry using C_{Dmax} until an arbitrarily selected time τ_s where the control is allowed to switch to C_{Dmin} instantaneously and maintain that value until exit. The exit state namely velocity and flight path angle must be such that the transfer orbit at exit will reach LEO at apoapse, or satisfy (2-3) of Appendix 2 for a given α_2. This can be achieved by varying the switch time τ_s until (2-3) is satisfied. Since the entry state or equivalently the target conic perigee of the deorbit ΔV_1 was held fixed, the procedure just described is repeated with a new entry state and the τ_s that satisfies (2-3) found again. As has been mentioned earlier the trajectory that results in the minimum ΔV_2 is then chosen to represent a near optimal transfer whose exit state can be used as the initial guess in the backward integration scheme in order to iterate on the overall optimal solution.

Results

The results of this study are presented in three parts. In the initial part, a series of ballistic or constant C_D fly-throughs are generated in order to establish the undershoot and overshoot boundaries and also to provide with a reference with which the optimal transfer can be compared and fuel savings determined.

In the second part, a seris of one switch C_{Dmax} - C_{Dmin} near optimal trajectories are presented from which the appropriate initial guesses required for the optimization scheme are directly obtained and finally an optimal transfer example is shown and compared with both the ballistic and single switch solutions.

The results that are presented in this study assumed a nominal atmosphere which is tabulated in Table 1 and obtained from Reference 7. The ballistic coefficient ($\beta = m/C_DA$) was assumed to have a minimum value of 25 kg/m^2. As such, a C_{Dmax} value of 3.0 was assumed. C_{Dmin}'s of 0.12, 0.30 and 1.0 were analyzed in this study. This range of C_D is consistent with conceptual designs utilizing drag modulation (Reference 1). One specific aeroassisted return from HEO was analyzed. This was geosynchronous return which gave us an entry speed of 10.31 km/sec at entry altitude of 120 km. This same altitude established the exit interface, as well.

Generation of Ballistic Flight Path

Tables 2, 3, 4, and 5 show the resultant orbits from ballistic flight in the atmosphere as a function of the de-orbit target perigee for ballistic coefficients of 625, 250, 75 and 25 Kg/m^2 (i.e., C_D = 0.12, 0.30, 1.0 and 3.0), respectively. This demonstrates the sensitivity of ballistic flight where approximately a 0.1 km error means the difference between aerobraking into a LEO (~ 200 km) or crashing. It shows that the target perigee in the de-orbit maneuver to ballistically aerobake into a 200 km LEO is approximately 6439.0, 6445.7, 6453.4 and 6459.7, respectively, for the four values of drag coefficient. Due to the sensitivity of the problem, these perigee altitudes can be considered the undershoot boundaries. The specific undershoot boundaries depend on the drag capability (i.e., C_{Dmax}/C_{Dmin} ratio). The ΔV_2 range to trim to a 200 km LEO is 82 to 72 m/sec, respectively, which indicates that as the ballistic coeffiecient decreases or C_D increases the ΔV_2 decreases.

Table 1 - Nominal Atmosphere Model

Altitude km	Density cm/cm^3	Pressure mbar	Speed of Sound m/sec	Temperature ^{o}k	Viscosity$_2$ nτ-sec/m^2
50	1.032E-6	8.006E-1	329.5	270.15	1.701E-5
55	5.610E-7	4.222E-1	324.5	262.15	1.661E-5
60	3.018E-7	2.172E-1	317.4	250.65	1.502E-5
65	1.601E-7	1.071E-1	306.1	233.15	1.511E-5
70	8.082E-5	5.003E-2	294.4	215.65	1.416E-5
75	3.850E-8	2.190E-2	282.2	198.15	1.318E-5
80	1.713E-8	8.881E-3	269.4	180.68	1.216E-5
85	6.672E-9	3.393E-3	266.8	177.07	1.196E-5
90	2.518E-9	1.295E-3	268.3	178.67	1.207E-5
95	3.715E-10	2.124E-4	282.9	192.98	1.324E-5
100	5.312E-11	4.904E-5	329.8	254.47	1.704E-5
116	2.368-11	2.602E-5	392.3	354.95	2.215E-5

Table 2

C_D = .12

r_p(km)	t_f(sec)	v_f(km/s)	γ_f(deg)	r_{a_f}(km)	ΔV_2(m/s)
6438.9	crashed				
6439.	601.06	7.776950	.895250	6542.632	82.407
6439.1	532.97	7.842947	1.308978	6665.963	89.486
6439.2	495.75	7.903303	1.591965	6838.870	127.959
6439.3	470.45	7.959373	1.811976	7023.864	173.444
6440.	388.99	8.279476	2.695264	8294.136	453.063
6442.	318.10	8.880892	3.645161	11755.570	923.945
6444.	288.26	9.275672	4.020852	15311.336	1175.436
6446.	269.87	9.555858	4.197319	18967.810	1319.300

Table 3

C_D = 0.3

r_p(km)	t_f(sec)	v_f(km/s)	γ_f(deg)	r_{a_f}(km)	ΔV_2(m/s)
6445.5	crashed				
6445.6	619.89	7.746398	.587651	6512.588	94.706
6445.7	517.35	7.822124	1.128311	6610.157	77.481
6445.3	473.60	7.889804	1.446190	6788.404	112.887
6445.9	446.00	7.951965	1.681997	6990.131	162.454
6446.	426.06	8.009885	1.871531	7194.240	212.645
6447.	341.48	8.458194	2.864588	9145.360	599.658
6446.	308.18	8.780921	3.317631	11044.902	850.042
6449.	287.83	9.037416	3.588734	12992.239	1027.796
6450.	273.55	9.245276	3.762002	14976.149	1156.356

Table 4

C_D = 1

r_p(km)	t_f(sec)	V_f(km/s)	γ_f(deg)	r_{a_f}(km)	ΔV_2(m/s)
6453.3	crashed				
6453.5	473.17	7.824095	1.063686	6605.799	72.863
6453.55	448.68	7.863745	1.239999	6702.345	89.596
6453.60	430.48	7.901335	1.385393	6813.852	115.568
6453.65	416.07	7.937229	1.510017	6930.457	144.458
6453.7	404.19	7.971690	1.619518	7048.619	173.964
6454.2	340.75	8.263866	2.314687	8208.965	432.152
6454.2	340.75	8.263866	2.314687	8208.965	432.152
6454.7	311.31	8.493445	2.696911	9321.206	624.937
6455.2	292.61	8.684921	2.950958	10417.311	775.532
6455.7	279.11	8.849420	3.133805	11512.757	896.798
6456.2	268.65	8.993291	3.271220	12615.064	996.260
6456.7	260.15	9.120678	3.377213	13728.322	1078.833
6457.2	253.01	9.234540	3.460310	14855.264	1147.978
6457.7	246.86	9.337178	3.526154	15998.845	1206.273
6458.2	241.44	9.430706	3.578889	17166.174	1255.837

Table 5

C_D = 3

r_p(km)	t_f(sec)	V_f(km/s)	γ_f(deg)	r_{a_f}(km)	ΔV_2(m/s)
6459.6	crashed				
6459.7	449.77	7.795463	.894869	6555.034	71.279
6459.8	399.59	7.889165	1.270910	6769.577	102.600
6459.85	384.24	7.931569	1.406846	6904.699	135.821
6459.9	371.97	7.971771	1.523306	7041.979	170.166
6460	353.14	8.046833	1.716403	7314.680	236.756
6460	251.39	8.957269	3.007160	12318.829	970.005
6463	234.75	9.228507	3.205316	14786.182	1142.822

Generation of Near Optimal Flight Path

Assuming the fixed C_{Dmax}-to-C_{Dmin} strategy, a number of trajectories were flown to various LEO's with altitudes in the range of 122 to 622 km using a fixed switching logic as discussed before. These are reflected in Figures 4, 5 and 6 for C_{Dmin}-C_{Dmax} pairs of (1, 3), (.3,3) and (.12, 3). The number adjacent to each parenthesis is the perigee radius plus 6400 km. Each curve corresponding to a given C_{Dmin}-C_{Dmax} pair is for a given target perigee r_p with each point of the curve corresponding to a different switching time τ_s. However the curves related to the purely ballistic cases or constant C_D are obtained by varying the target perigee r_p, using the data displayed in tables 2,3,4 and 5. These figures show that for a given apogee radius r_a corresponding to a LEO orbit, several combinations of r_p and switch times are possible but that only one such set will lead to the minimum ΔV_2 value. Furthermore, as the C_D range gets larger, the ΔV_2 savings with respect to the purely ballistic case become larger for given low LEO's. Included in each Figure are the corresponding ballistic trajectory results. Essentially reflected in these figures are the ΔV_2 minimum for each C_{Dmax}-to-C_{Dmin} trajectory to a given LEO as a function of the perigee altitude. At apogee altitudes of 500 km or greater, the differences due to a ballistic trajectory, and perigee altitude become insignificant. LEO's at altitudes of about 200 km reach a minimum ΔV_2 for high perigee altitude or shallow entry which corresponds to operating in the overshoot boundary. At the more reasonable LEO of about 350 km, as expected, the effect of perigee altitude is somewhat desensitized with the modulated drag trajectory giving the ΔV_2 minimum solution.

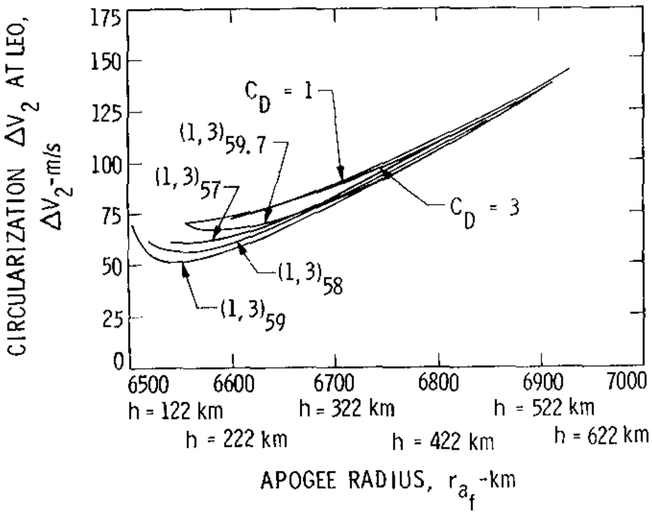

Figure 4

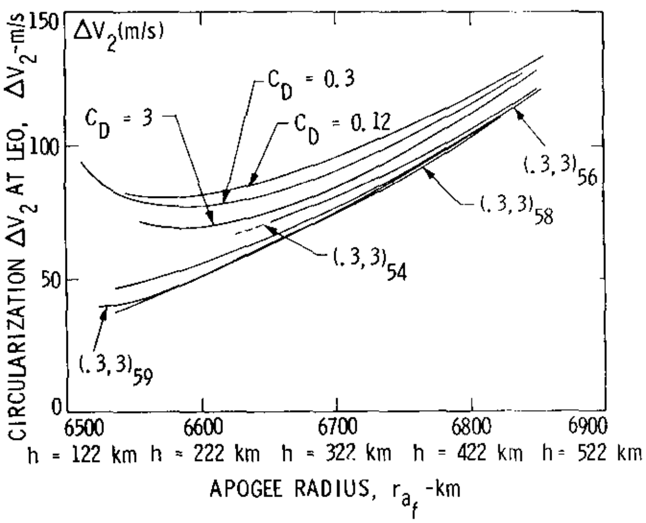

Figure 5

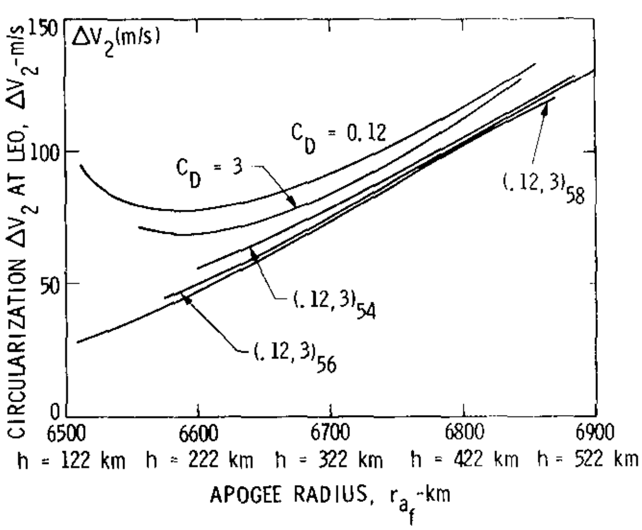

Figure 6

Figure 7 shows the variation of the critical switching time t_s (latest possible switching time) with target altitude for different C_D intervals. For a given C_{Dmin}-C_{Dmax} interval, t_s increases with h and for a given target h, t_s increases with the C_D interval. Each point on these curves has a corresponding achieved LEO associated with it. It demonstrates that shallower entry allows for greater flexibility. A 1.0 km variation corresponds to approximately 0.1° variation in entry flight path angle.

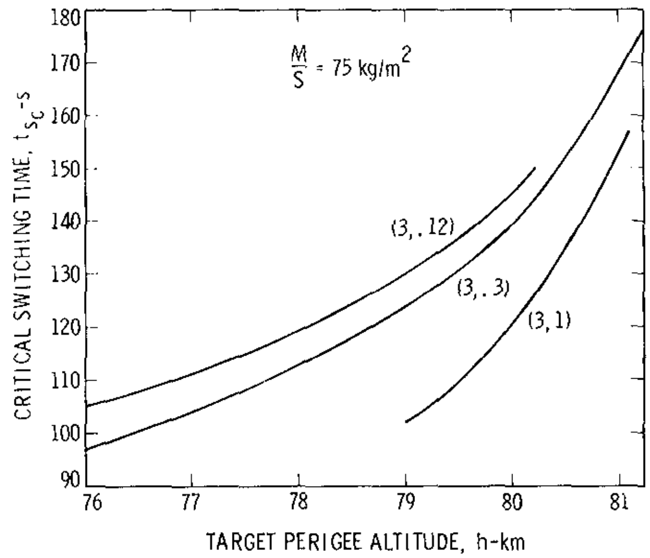

Figure 7

A specific LEO of 246.5 km was examined corresponding to a target altitude h = 80 Km with a switch from C_{Dmax} = 3 to C_{Dmin} = .12 at time t_s = 144 sec after entry. The general response is shown in Figures 8 which shows altitude, velocity, flight path angle and time histories of the trajectory. This trajectory flew extensively at C_{Dmax} with a switch near the last 0.400 km/sec aerobrake. This of course was due to the shallow entry which operated near the overshoot boundary for this LEO. The control capability was also very great (C_{Dmax}-to-C_{Dmin} ratio of 25:1). The ΔV_2 was approximately 53 m/s.

Figure 8 shows that at entry, a slight increase in velocity takes place due to the presence of a small gravity component along the velocity vector. Severe deceleration of the order of 3 g's takes place at the 85 Km mark with the vehicle at C_{Dmax}. The instantaneous switch to C_{Dmin} pulls the spacecraft out of the atmosphere with little velocity depletion taking place after the switch, failure to switch resulting in a crash.

Finally, as opposed to the constant C_D fly throughs in which the altitude versus time curve is almost symmetrical, the minimum of h is now much closer to entry time.

Generation of Optimal Flight Path

The technique of backward integration of Appendices 1 and 2 is applied to the C_{Dmax}-C_{Dmin} trajectory of the previous section, in order to generate the optimal flight path. The C_{Dmax}-C_{Dmin} trajectories are either optimal or near optimal since it is not expected to encounter more than one or at most two switches in the control variable C_D between its max and min values.

Furthermore the exit state, namely v_f and s_f obtained from these one-switch trajectories provide an excellent initial guess (s_f in the backward integration case) to search for the optimal solution. For the case where only ΔV_2 is minimized (see Appendix 2 for the minimum $\Delta V_1 + \Delta V_2$ case) the iteration is carried on s_f and λ_h until the given entry state (v_e, s_e) is recovered.

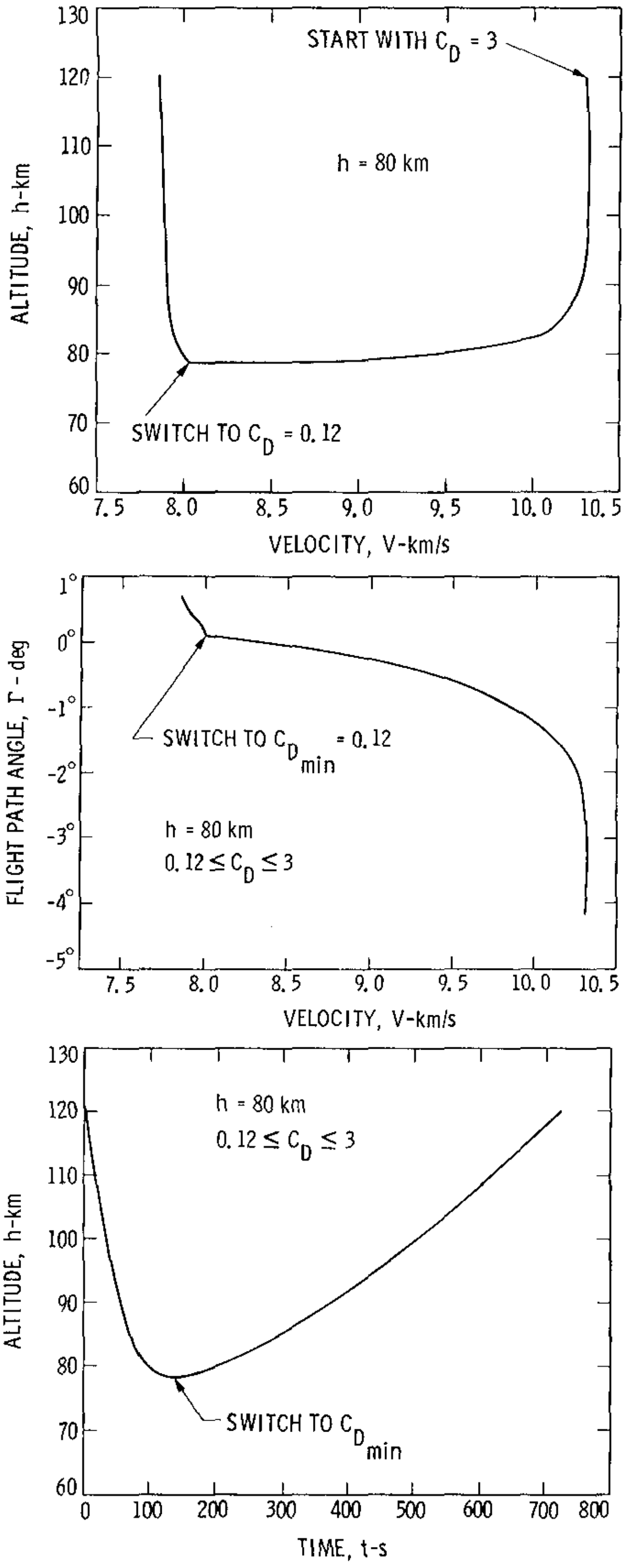

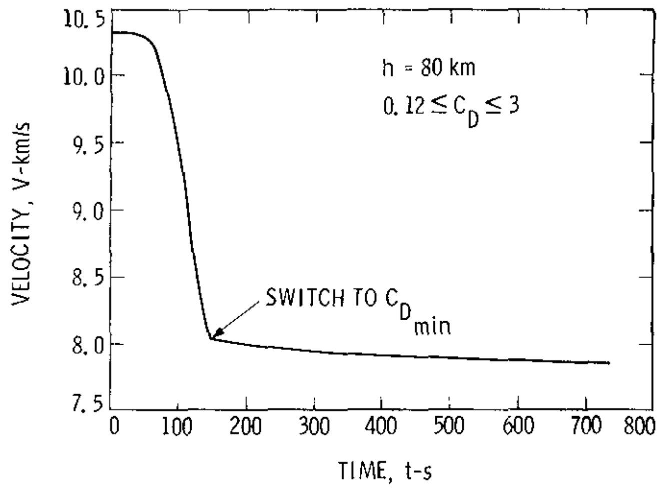

Figure 8

The switches are carried out according to the changes in sign of λ_v (Figure 9) and the optimal path generated consists of a $C_{min}-C_{Dmax}-C_{Dmin}$ strategy with the first switch taking place at t_s = 35.879 sec, the second switch at t_s = 145.879 sec and the total atmospheric flight time t_f = 723.600 sec. This optimal (minimum ΔV_2) trajectory is some 11.121 sec longer than the near optimal one-switch example of the previous section and the ΔV_2 needed to circularize is some 0.5 m/s less. This trajectory is reflected in Figure 10 which includes altitude, velocity, dynamic pressure and convective heating rate (1 meter sphere) time histories. The modification to the trajectory was slight since the C_{Dmin} initial flight was very brief and the velocity depletion is still taking place during the C_{Dmax} portion of the path.

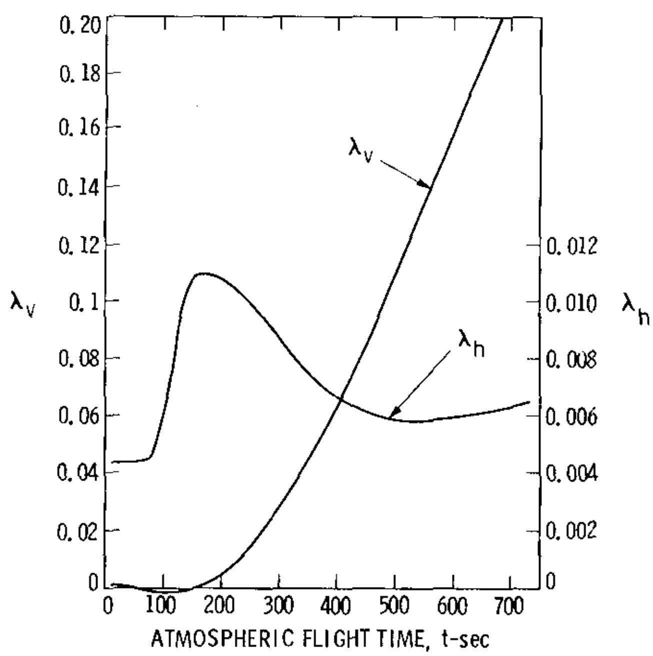

Figure 9

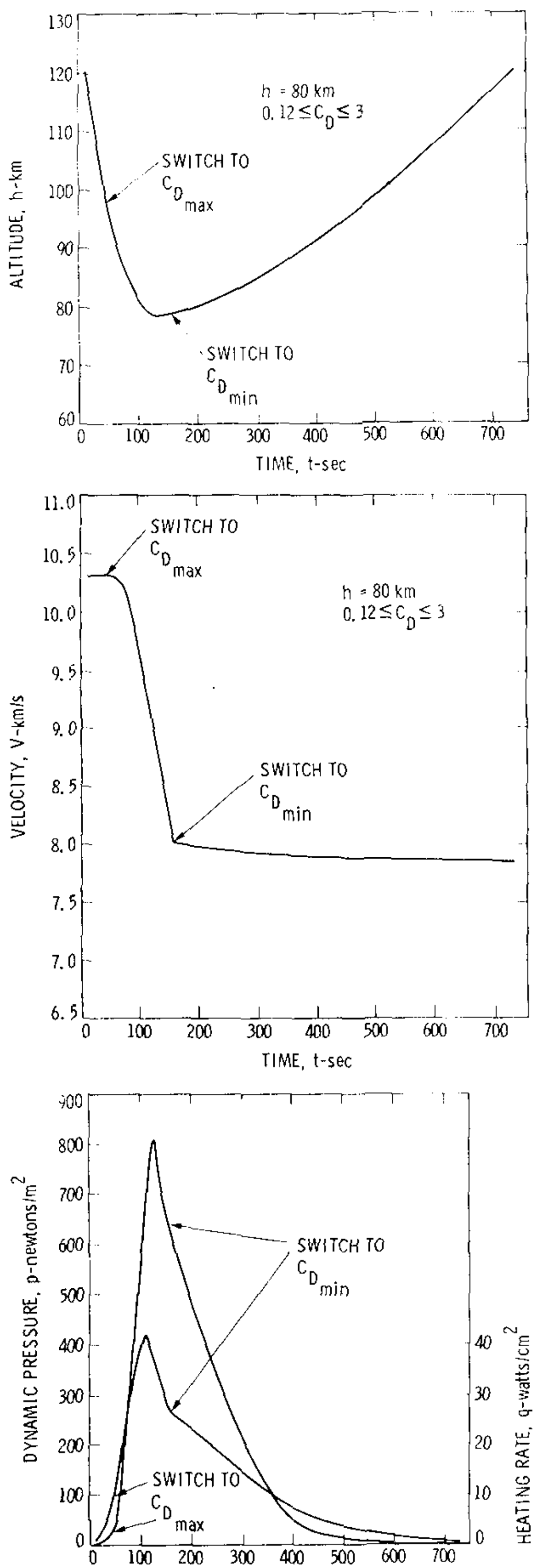

Figure 10

Discussion of Closed Guidance

The optimal orbital transfer study suggested that the nature of the atmospheric flight trajectory control would be bang-bang between a C_{Dmax} and C_{Dmin}. Of the two trajectories solved, one resulted in an optimal orbit transfer. The first suggested that only one switch would occur from initial flight at C_{Dmax} to a final switch to C_{Dmin} to effect a skip trajectory. Unfortunately, this is essentially a ballistic trajectory which does not provide the accuracy control required to make drag modulation a feasible concept. The latter strategy resulted in two switches from C_{Dmin}-to-C_{Dmax}-to-C_{Dmin}. This solution is a slight modification of the C_{Dmax}-to-C_{Dmin} trajectory, since the initial flight at C_{Dmin} is relatively short. These solutions were a result of the mathematically derived optimality condition which constrained the atmospheric trajectory to exit at C_{Dmin}.

The guidance mechanization that follows suggests an additional solution with a C_{Dmax}-to-C_{Dmin}-*to*-C_{Dmax} *strategy. It turns out that the* difference in orbit trim ΔV between this strategy and the two discussed above is on the order of meters per second.

This strategy, though, has the added advantage of providing significant accuracy control capability, since it can readily modify *the ballistic entry trajectory.* This will be demonstrated in the discussion of the results.

Before discussing the guidance approaches and results, it is important that the definition of C_{Dmax} and C_{Dmin} strategies be made as it relates to guidance. In the optimal orbital transfer analysis, the trajectory was shaped by bang-bang control as dictated by the Maximum Principle. In the guidance analysis, the trajectory is not absolutely controlled in a bang-bang mode, but rather commands are issued at intermediate values of C_{Dmax}-to-C_{Dmin}. This allows the trajectory to be trimmed and damped through various phases as will be discussed. The trajectory, though, does *reside at some* C_{Dmax} *and* C_{Dmin} values *through* a large portion of the trajectory. As such, the reference to C_{Dmax}-C_{Dmin} and C_{Dmax}-C_{Dmin}-C_{Dmax} guidance strategies is made.

C_{Dmax}-C_{Dmin} Guidance

The strategy here is for the entry vehicle to *fly initially at its* C_{Dmax} *or* β_{min} *configuration* until some reference drag acceleration (D_{Ref}), has been exceeded. The entry vehicle is then commanded to change its configuration to a commanded β_c to fly this reference drag acceleration. The reference β, which usually tends toward a C_{Dmin} or β_{max} is based on a *value which will insure skip-out at a desired exit* speed and flight path angle. The entry vehicle continually modulates its configuration to this D_{Ref} until it meets a skip or exit state criteria. Once this criterion has been met, it flies at its current configuration until exit. This is usually at the β_{max} command in the trajectory.

The criterion used to initiate exit is given as follows if

$V_e^1 \leq V_e$ then the criterion has been met.

where V_e = the desired exit speed

$$V_e^1 = V \exp(-k) \qquad (8)$$

V = current air speed

$$k = \frac{H_s D}{\beta_c \gamma_m V^2} \qquad (9)$$

D = measured drag acceleration

γ_m = mean value of exit flight path angle

H_s = density scale height
β_c = the current commanded β

This is derived in Appendix 3 and also assumes that for this strategy (HE-H)>>Hs. If the criterion $V_e^1 \leq V_e$ is not met, a new command is issued based on a skip criterion damped by the D_{Ref} controller. This is mechanized as follows

$$\beta_c = \beta_{Ref} + C_1(D-D_{Ref}) - C_2(\dot{H} - \dot{H}_{Ref}) \qquad (10)$$

where

$$\beta_{Ref} = \frac{q H_s}{k_{Ref} \gamma V^2} \qquad (11)$$

q = $D\beta_c$, inferred dynamic pressure

β_c = previous command

$\dot{H}$ = computed rate of climb

$$\dot{H}_{Ref} = -\frac{2Hs\ D_{Ref}}{V} \qquad (12)$$

$C1, C2$ = Guidance gains

$$k_{Ref} = \ln(V/_{Ve}) \qquad (13)$$

A derivation of the guidance gains is given in Appendix 4 and the reference quantities are derived in Appendix 3.

In general, the criterion on Ve is slightly biased from the exact exit air speed which is due to the differences between the linearized maneuver and actual flight dynamics.

C_{Dmax}-C_{Dmin}-C_{Dmax} Guidance

This strategy is a modification of the C_{Dmax}-C_{Dmin} strategy which adds one more degree of control. Once C_{Dmax}-C_{Dmin} approach has met its criteria, it will exit the β controller at its last β command. In essence, it has no more control over the trajectory. The intent of the modification is to continue to modify or correct the exit maneuver. It does this by continuing to issue β commands without damping. These commands are executed as follows

$$\beta_c = \frac{q H_s}{k_c \dot{H} V} \qquad (14)$$

where

$$k_c = \frac{\ln(V/_{VE})}{1 - \exp\frac{(H - HE)}{H_s}} \qquad (15)$$

HE = exit altitude
H = current computed altitude
$q = D\beta_c$, again dynamic pressure inferred from previous β command

The general response of this modification is to command β to β_{max} or C_{Dmin} shortly after the C_{Dmax}-C_{Dmin} mode has been exited and later command β to β_{min} or C_{Dmax}. This is due to the lack of damping in the guidance mechanizations. Correction to this response is a future task. As the entry vehicle climbs, the density diminishes and as such the exit is towards C_{Dmax} or β_{min} for final correction. These commands are issued until the entry vehicle drag drops below 0.1 g's.

Results

The above guidance strategies and mechanizations were implemented into a flight dynamics, and Guidance, Navigation and Control simulation which decouples the various functions (Reference 6). A number of parametric guidance and error analyses were then performed to determine performance.

The entry vehicle was assumed to have a β_{min} = 25 kg/m^2 and potential to modulate its β to C_{Dmax}-to-C_{Dmin} ratios of 25:1, 10:1 and 3:1. This is consistent with some proposed concepts (i.e. Reference 2).

For these analyses, the orbit transfer considered was a return from geosynchronous orbit to a 350 km LEO. This corresponds to an entry speed of about 10.31 km/sec (inertial) and 9.84 (air relative). The nominal atmospheric model is that given in Table 1 and Reference 7.

Entry Flight Path Angle Sensitivity Analysis

Sensitivity analyses of the exit state as a function entry flight path angle were performed using the two guidance strategies. The intent here was to determine the entry corridor for a geosynchronous to LEO return mission and determine how wide it was for each guidance strategy. This is indiated in Figure 11 for an entry configuration with C_{Dmax}-to-C_{Dmin} ratio capability of 25:1. As will be noted, an inflection in the exit speed and entry flight path angle curve is observed for the C_{Dmax}-C_{Dmin} guidance strategy which suggests that an improvement over the ballistic trajectory can be made (Reference 5) by this approach. The C_{Dmax}-C_{Dmin}-C_{Dmax} guidance strategy, though, gives the superior performance. The exit state sensitivity over $\pm$ 0.2° in entry flight path angle is essentially zero. The ΔV required to trim errors about a -4.8° nominal (ΔV = 106 m/sec) is on the order of $\pm$ 10 m/sec. The entry at -5.0° results in exit states very close to the optimal trajectory and trim ΔV differences on the order of 2 m/sec.

Atmospheric Density Dispersion Sensitivity Analysis

Sensitivity analyses of the exit state to variation in atmospheric density were performed

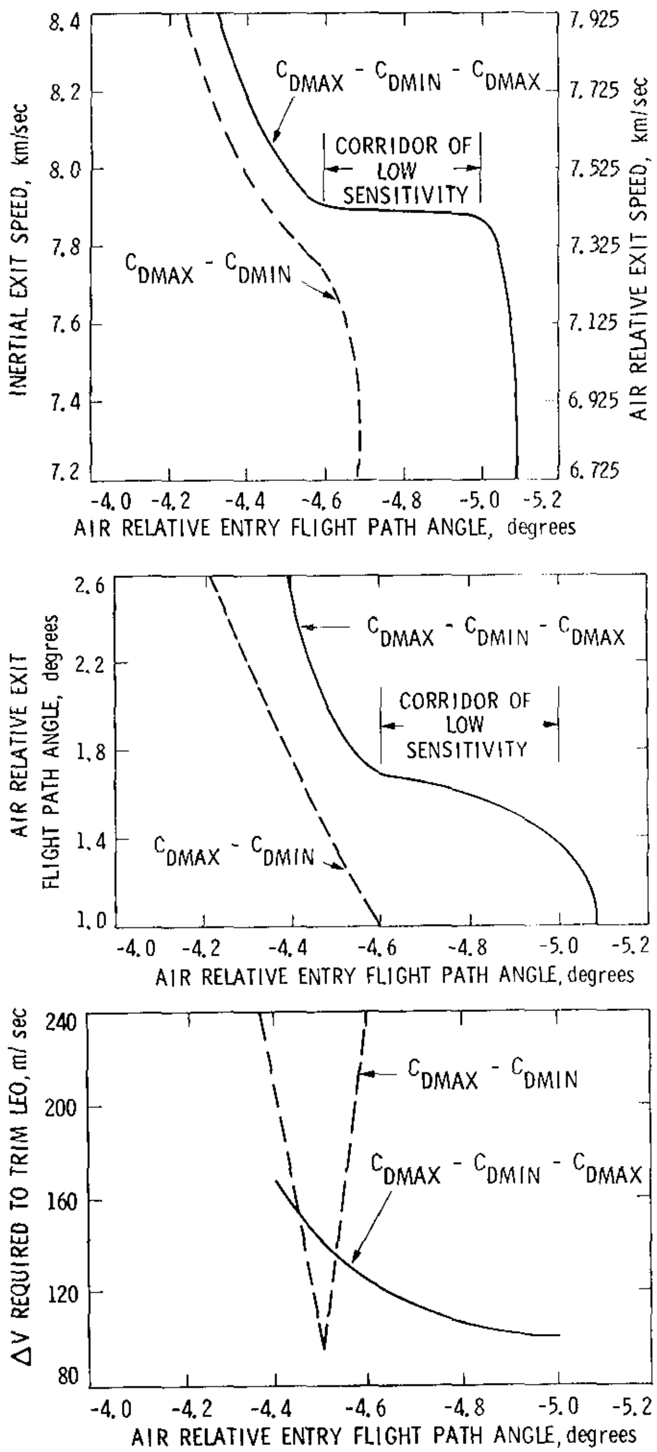

Figure 11

using the two guidance strategies. This is reflected in Figure 12. The nominal atmospheric model was perturbed in increments of 15% by a multiplier which essentially assumes that the entire atmosphere density profile is off nominal by a fraction. Trajectories were simulated using the nominal entry condition derived from the prior entry corridor analysis. Nominal entry was -4.5° and -4.8° for the C_{Dmax}-C_{Dmin} strategy, C_{Dmax}-C_{Dmin}-C_{Dmax} strategy. Again, the C_{Dmax}-C_{Dmin}-C_{Dmax} strategy provided the superior performance with essentially zero sensitivity and was extremely adaptive. In view of the prior

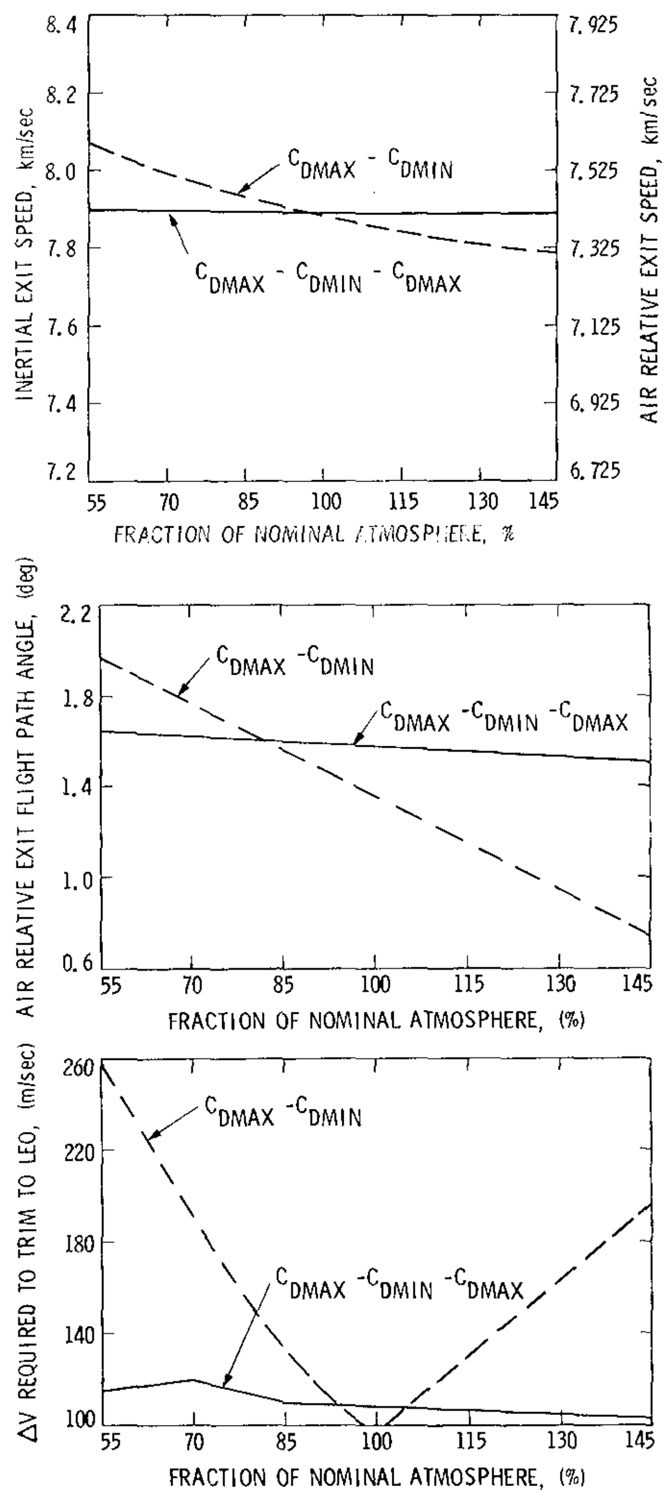

Figure 12

sensitivity analysis, this should not be surprising, since a 50% dispersion in density is approximately equivalent to a 0.1° entry flight path angle dispersion (Reference 4). Also, this assumes a C_{Dmax}-C_{Dmin} ratio of 25:1. Figure 13 shows time histories of the trajectories for these dispersions.

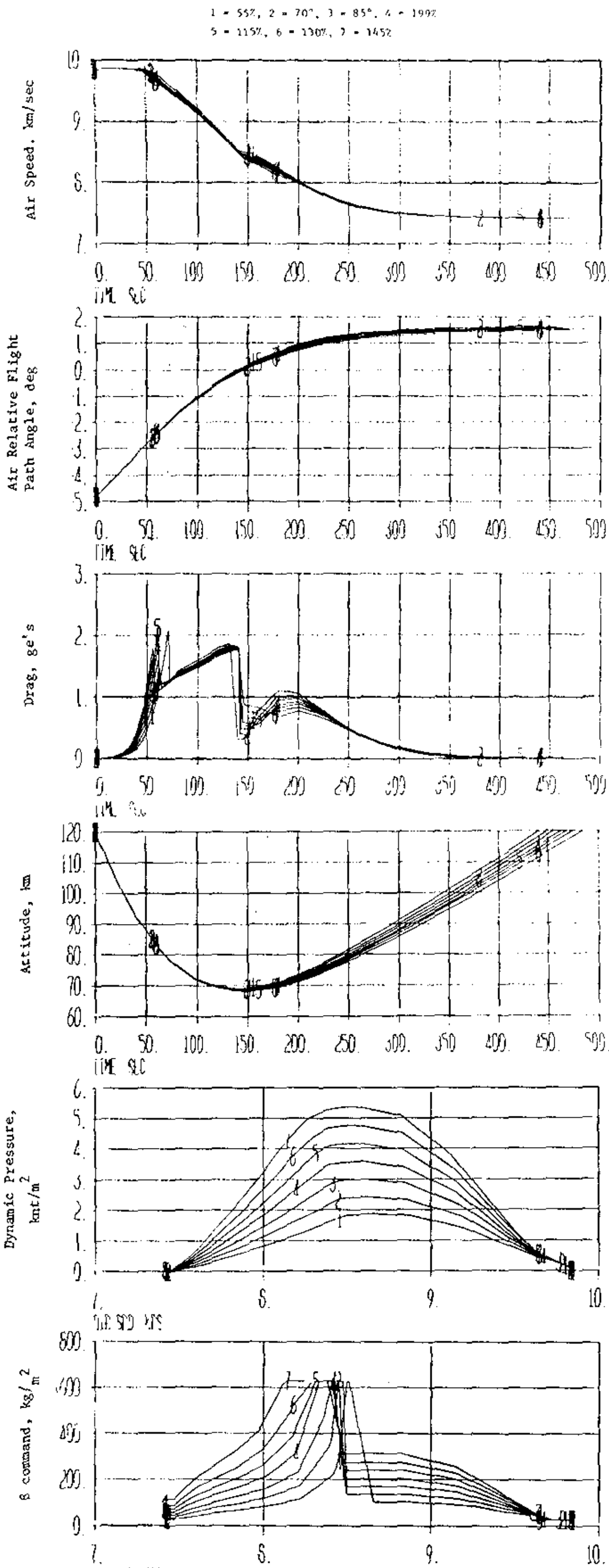

Figure 13

Sensitivity to Lift and Drag Dispersions

The response of the C_{Dmax}-C_{Dmin}-C_{Dmax} guidance mechanization to lift was investigated to determine its capability to control unforeseen aerodynamic forces. Simulations were executed for an L/D range of −0.1 to 0.1 at nominal entry of −4.8°. The flight dynamic simulation, which feeds back acceleration and velocity information to the guidance and navigation function, simulated the presence of lift. The guidance and navigation functions based on trajectory response attempted to correct the bias. Figure 14 shows the guidance sensitivity. It can be insensitive to small lift biases, but falls off the edge and crashes for an L/D nose down of more than 0.03. This is 10% of that experienced by Apollo type entry vehicles. This could potentially be a problem. The entry vehicle will probably require very active pitch damping or roll control.

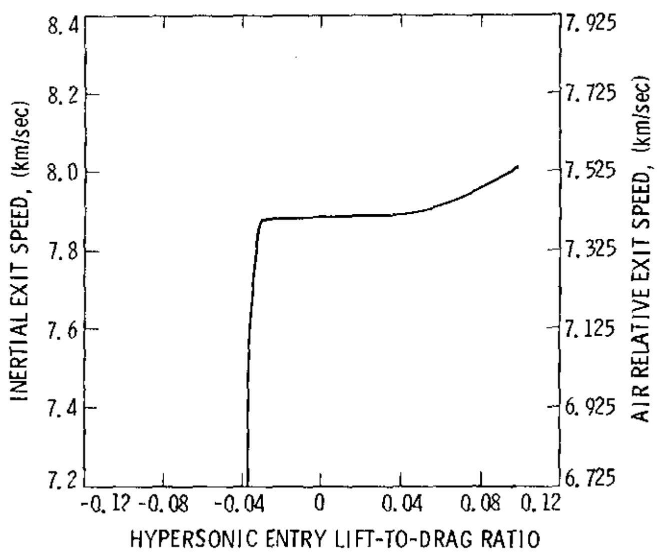

Figure 14

In addition, dispersions of ± 20% in drag were simulated to again test the adaptiveness of the mechanization. The response or sensitivity to error in drag over nominal was essentially zero. Of course, this was for the C_{Dmax}/C_{Dmin} ratio of 25:1 which is a great deal of control capability.

Entry Flight Path Angle and Control Sensitivity Analysis

The sensitivity analysis shown in Figure 11 was repeated for various values of C_{Dmax}-to-C_{Dmin} control ratios using a C_{Dmax}-C_{Dmin}-C_{Dmax} guidance strategy. This is shown in Figure 15. As can be noted, C_{Dmax}-to-C_{Dmin} ratios of less than 10:1 significantly reduces the exit state control capability. Based on atmospheric dispersions and entry state navigation, an entry corridor width of ± 0.1° should be maintained. This suggests control authority requirements of 10:1 or better.

Accuracy Assessment

An accuracy assessment of the C_{Dmax}-C_{Dmin}-C_{Dmax} guidance strategy and mechanization was performed for a C_{Dmax}-to-C_{min} control ratio of

Table 6 - Aeroassisted Orbital Transfer Accuracy for a C_{DMAX}-C_{DMIN}-C_{MAX} Guidance Mode and a C_{DMAX}-to-C_{DMIN} Ratio of 25:1

Input Error Source				3σ Output Error						
Parameter	Description	Value, 3σ	Units	Exit Speed, m/sec	Exit Flight Path Angle, deg	Apoapsis Altitude, km	Orbit Period, sec	Great Circle Arc, deg	Corrective ΔV over nominal for LEO, m/sec	Error Type*
L/D	Lift-to-Drag Ratio Uncertainty	0.03	—	3	0.27	32.	8.	7.9	10	Pert-Nom
C_D	Drag Coefficient Uncertainty	20	%	0.	-0.03	-3.	0.	0.4	0	Pert-Nom
γ_a	Entry Flight Path Control	0.20	deg	24.	0.10	72.	49.	-3.5	18.	Pert-Nom
ρ	Density Uncertainty	45	%	-1.	-0.07	-9.	-4.	1.3	4.	Pert-Nom
u	Knowledge of Entry Position – Downtrack	1000	m	4	0.07	7	4.	1.8	4.	Nav-Perb
v	– Crosstrack	1000	m	-3	0.07	7	0.	1.5	3.	Nav-Perb
w	– Vertical	1000	m	0	0.07	9	4.	1.3	4.	Nav-Perb
$\dot{u}$	Knowledge of Entry Velocity – Downtrack	1	m/sec	-2	0.08	9	0.	1.3	4.	Nav-Perb
$\dot{v}$	– Crosstrack	1	m/sec	-3	0.07	6	0.	1.5	3	Nav-Perb
$\dot{w}$	– Vertical	1	m/sec	-4	0.08	7	4.	1.5	3.	Nav-Perb
EV	Initial Gyro Misalignment	0.053	deg	-3	0.07	6	0.	1.5	3.	Nav-Perb
GCDR	Gyro Acceleration Insensitive Drift Rate	0.04	deg/hr	-2	0.07	6	0.	1.5	3.	Nav-Perb
GIA	Gyro Acceleration Sensitive Drift Rate – Input Axis	0.04	deg/hr/g	-3	0.07	6	0.	1.5	3	Nav-Perb
GSA	Gyro Acceleration Sensitive Drift Rate – Spin Axis	0.04	deg/hr/g	-3	0.07	6	0.	1.5	3.	Nav-Perb
HISA	Gyro Anisoelasticity	0.03	$deg/hr/g^2$	-3	0.07	6	0.	1.5	3.	Nav-Perb
B	Accelerometer Bias	5	μg	-3	0.07	6	0.	1.6	3.	Nav-Perb
SF	Accelerometer Scale Factor	0.1	%	-2	0.07	-1	-4	2.4	1.	Nav-Perb
Q	Accelerometer Non-Linearity	0.01	%/g	-3	0.07	6	0	1.5	3.	Nav-Perb
AMLT	Accelerometer Misalignment	0.053	deg	-2	0.05	4	4	1.2	2.	Nav-Perb
		3σ RSS		27	0.40	83	51.	10.5	24.	RSS

*Nom – Nominal Case State
Pert – Perturbed Case State
Nav – Navigated State
Perb – Nominal Case State perturbed by navigator error

Table 7 - Aeroassisted Orbital Transfer Trajectory Bias to Navigator Errors

Input Error Source				3σ Output Error						
Parameter	Description	Value, 3σ	Units	Exit Speed, m/sec	Exit Flight Path Angle, deg	Apoapsis Altitude, km	Period, sec	Great Circle Arc, deg	Corrective ΔV over nominal for LEO, m/sec	Error Type*
u	Knowledge of Entry Position – Downtrack	1000	km	0.	-0.03	-5.	-4.	-0.2	2	Perb-Nom
v	– Crosstrack	1000	km	0.	-0.02	-4.	-4.	0.0	1	Perb-Nom
w	– Vertical	1000	km	0.	-0.02	-4.	-4.	0.0	1	Perb-Nom
$\dot{u}$	Knowledge of Entry Velocity – Downtrack	1	m/sec	-1.	-0.03	-7.	-4.	0.4	2	Perb-Nom
$\dot{v}$	– Crosstrack	1	m/sec	0.	-0.02	-4.	-4.	0.0	1	Perb-Nom
$\dot{w}$	– Vertical	1	m/sec	0.	-0.03	-7.	-4.	-0.1	1	Perb-Nom
EV	Initial Gyro Misalignment	0.053	deg	0.	-0.02	-4.	-4.	0.0	1	Perb-Nom
GCDR	Gyro Acceleration Insensitive Drift Rate	0.04	deg/hr	-1.	-0.02	-4.	-4.	0.0	1	Perb-Nom
GIA	Gyro Acceleration Sensitive Drift Rate – Input Axis	0.04	deg/hr/g	0.	-0.02	-4.	-4.	0.3	1	Perb-Nom
GSA	Gyro Acceleration Sensitive Drift Rate – Spin Axis	0.04	deg/hr/g	0.	-0.02	-4.	-4.	0.0	1	Perb-Nom
HISA	Gyro Anisoelasticity	0.03	$deg/hr/g^2$	0.	-0.02	-4.	-4.	0.0	1	Perb-Nom
B	Accelerometer Bias	5	μg	0.	-0.02	-4.	-4.	0.0	1	Perb-Nom
SF	Accelerometer Scale Factor	0.1	%	2.	-0.01	4.	-4.	-1.0	2	Perb-Nom
Q	Accelerometer Non-linearity	0.01	%/g	0.	-0.02	-4.	-4.	0.0	1	Perb-Nom
AMLT	Accelerometer Misalignment	0.053	deg	0.	-0.02	-3.	-4.	-0.1	1	Perb-Nom

*Nom – Nominal Case State
*Perb – Nominal Case State perturbed by navigator error

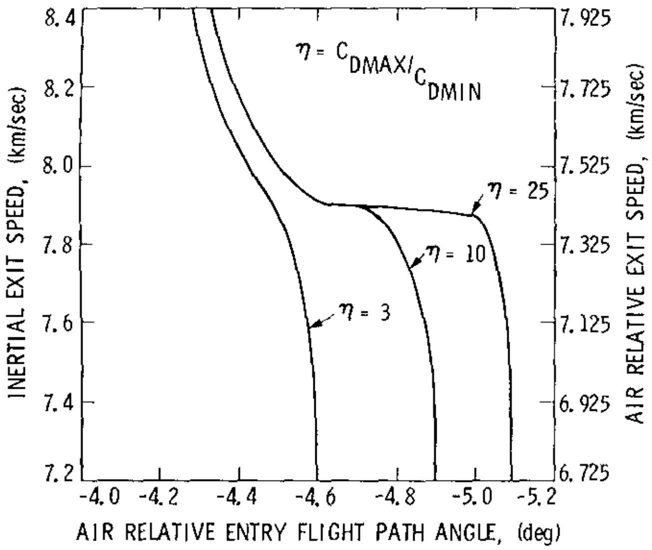

Figure 15

25:1. This is reflected in Table 6. It includes a number of navigation and control error sources which impact guidance performance. It points out that the driving error sources are in control of L/D and flight path angle. The corrective ΔV required is not excessive ($3\sigma\Delta V$ = 24 m/sec over the nominal ΔV of approximately 106 m/sec for a 350 km LEO). Additional Δ V, though, may be required to correct rendezvous phasing with 10.5^o great circle arc errors. These errors may be greater for entry vehicles with $C_{D_{max}}$-to-$C_{D_{min}}$ control capability of 10:1 or less. Table 7 shows the bias error between the actual state perturbed by the navigation and the actual nominal state.

Summary and Conclusions

An approach which efficiently searches out optimal aeroassisted orbital transfer has been developed. An explicit and adaptive closed loop guidance approach has also been developed with performance near the optimal and significant guidance accuracy. System design requirements have evolved from these studies which suggest that the entry system have $C_{D_{max}}$-to-$C_{D_{min}}$ control greater than 10:1 and never develop lift during the entire entry.

Acknowledgement

The research described in this paper was carried out by the Jet Propulsion Laboratory under contract with the National Aeronautics and Space Administration.

References

1. Andrews, D. G. and Bleotscher, F., 'Aerobraked Orbital Transfer Vehicle Definition,' AIAA Paper No. 81-0279, AIAA 9th Aerospace Sciences Meeting, Jan. 1

2. Cruz, M. I., French, J. R., and Austin, R. E., 'System Design Concepts and Requirements for Aeroassisted Orbital Transfer Vehicles', AIAA Paper No. 82-1379, AIAA 9th Atmospheric Flight Mechanics Conference, August, 1982, San Diego, CA.

3. J. A. Kechichian, N. X. Vinh, E. A. Rinderle, M. I. Cruz, 'Optimal Nonlifting Aeroassisted Transfer Between Coplanar Circular Orbits Using Drag Modulation', JPL Document 314-280, 25 August 1982.

4. M. I. Cruz, 'Drag Modulated Aeroassisted Orbital Transfer Guidance Studies', JPL Document 314-281, 15 September 1982.

5. Kechichian, J. A. and Rinderle, E.A., 'Sensitivity Analysis of De-orbit from High Altitude,' JPL Document 314.4-239, 1982.

6. Cruz, M. I. and Rinderle, E. A., 'ATMOS Analysis Computer Program,' JPL Document 725-76, March, 1982.

7. 'U. S. Standard Atmosphere Supplements,' 1966.

8. Cruz, M. I. and Rinderle,E.A., 'Aeroassisted OTV Ballistic Entry Sensitivity Analysis', JPL Document 314-267, 18 March 1982.

APPENDIX 1

FORMULATION OF THE OPTIMAL CONTROL PROBLEM

The exact equations of motion for a planar nonlifting entry into Earth's atmosphere are given by

$$\dot{V} = -\frac{1}{2}\rho\frac{S}{m}C_D V^2 - g s_\Gamma \qquad (1\text{-}1)$$

$$\dot{\Gamma} = -\frac{g}{V}c_\Gamma + \frac{V}{r}c_\Gamma \qquad (1\text{-}2)$$

$$\dot{H} = \dot{r} = V s_\Gamma \qquad (1\text{-}3)$$

where V, Γ and r are the velocity, flight path angle and radial distance respectively and where ρ, S, C_D and m are the air density, vehicle cross sectional area, coefficient of drag and vehicle mass. Finally $g(r) = \mu/r^2$ is the acceleration of gravity with μ the gravitational constant of Earth. In addition, r = H+R with R representing the radius of Earth and H altitude.

The atmosphere being assumed to have a radius R_a, a set of non-dimensional variables may be used to carry out the analysis of this problem.

$$\Gamma, \quad v = \frac{V}{\sqrt{\mu/R_a}}, \quad h = \frac{H}{H_e}, \quad \tau = \frac{t}{H_e}\sqrt{\frac{\mu}{R_a}} \qquad (1\text{-}3^1)$$

Using data from a tabulated standard atmosphere, let $\rho(H)$ represent the density at altitude H such that with ρ_o corresponding to sea level,

$$\delta(H) = \frac{\rho}{\rho_o} \qquad (1\text{-}4)$$

$$\frac{d\delta}{dh} = \frac{d\delta}{dH}\frac{dH}{dh} = \frac{H_e}{\rho_o}\frac{d\rho}{dH} \qquad (1\text{-}5)$$

where $\frac{d\rho}{dH}$ is the density gradient read from the table. The exact equations of motion (1-1) are then reduced to the dimensionless form below

$$\frac{dv}{d\tau} = -B\delta C_D v^2 - \frac{k}{(k-1+h)^2} s_\Gamma \qquad (1\text{-}6)$$

$$\frac{d\gamma}{d\tau} = \frac{c_\Gamma}{(k-1+h)} \left[v - \frac{k}{(k-1+h)v} \right] \qquad (1\text{-}7)$$

$$\frac{dh}{d\tau} = v s_\Gamma \qquad (1\text{-}8)$$

$$\text{where} \quad B = \frac{\rho_o S H_e}{2m} C_{Dmax} \quad \text{and} \quad k = \frac{R_a}{H_e} \qquad (1\text{-}8^1)$$

are factors depending on the physical characteristics of the vehicle and the atmosphere.

Replacing $\sin\Gamma$ by s, and introducing $\eta = C_D/C_{Dmax}$ with $\eta_{min} \le \eta \le 1$, the system equations reduce to

$$\frac{dv}{d\tau} = -B\delta\eta v^2 - \frac{ks}{(k-1+h)^2} \qquad (1\text{-}9)$$

$$\frac{ds}{d\tau} = \frac{(1-s^2)}{(k-1+h)} \left[v - \frac{k}{(k-1+h)v} \right] \qquad (1\text{-}10)$$

$$\frac{dh}{d\tau} = vs \qquad (1\text{-}11)$$

The Hamiltonian is then given by

$$H = \lambda_v \left[-B\delta\eta v^2 - \frac{ks}{(k-1+h)^2} \right] + \lambda_s \left[\frac{(1-s^2)}{(k-1+h)} \left\{ v - \frac{k}{(k-1+h)v} \right\} \right] + \lambda_h vs \equiv 0 \qquad (1\text{-}12)$$

The system being autonomous and the time of flight free, H=0 identically. Instead of minimizing Γ_f, it is possible to maximize v_f for given s_f and for $h_e=h_f=1$ with v_e and s_e also given.

H is then maximized by choosing C_D the control such that

$\lambda_v < 0$	$C_D = C_{Dmax}$
$\lambda_v > 0$	$C_D = C_{Dmin}$
$\lambda_v = 0$	C_D = intermediate

The Euler-Lagrange equations are given by

$$\frac{d\lambda_v}{d\tau} = 2\lambda_v B\delta\eta v - \frac{\lambda_s(1-s^2)}{(k-1+h)} \left[1 + \frac{k}{(k-1+h)v^2} \right] - \lambda_h s \qquad (1\text{-}13)$$

$$\frac{d\lambda_s}{d\tau} = \lambda_v \frac{k}{(k-1+h)^2} + \frac{2s\lambda_s}{(k-1+h)} \left[v - \frac{k}{(k-1+h)v} \right] - \lambda_h v \qquad (1\text{-}14)$$

$$\frac{d\lambda_h}{d\tau} = \lambda_v B\eta v^2 \frac{d\delta}{dh} + \frac{\lambda_s(1-s^2)}{(k-1+h)^2} \left[v - \frac{2k}{(k-1+h)v} \right] - \frac{2k\lambda_v s}{(k-1+h)^3} \qquad (1\text{-}15)$$

The intermediate control case can be ruled out by observing that for $\lambda_v=0$, $\frac{d\lambda_v}{d\tau} = 0$, the Hamiltonian in (1-12) and the equation (-13) are satisfied only if $\lambda_s = \lambda_h = 0$ too.

APPENDIX 2

A DISCUSSION OF THE TRANSVERSALITY CONDITIONS

Let r_1 represent the radius of the high orbit and r_2 the radius of LEO.

With $\alpha_1 = {}^{r_1}/R_a$ and $\alpha_2 = {}^{r_2}/R_a$ and $\Delta v = \frac{\Delta V}{\sqrt{\mu/R_a}}$, the conservation of the angular momentum gives

$$v_1 = \frac{v_e c_{\Gamma e}}{\alpha_1} \quad ; \quad v_2 = \frac{v_f c_{\Gamma f}}{\alpha_2} \qquad (2\text{-}1)$$

where v_1 represents the nondimensional velocity at HEO just after the application of the deorbit Δv_1 and Δv_2 represents the velocity just before the application of the circularizing ΔV_2 at LEO. v_e, s_e and α_1 are related by

$$(2-v_e^2)\alpha_1^2 - 2\alpha_1 + v_e^2(1-s_e^2) = 0 \qquad (2\text{-}2)$$

while v_f, s_f and α_2 satisfy

$$(2-v_f^2)\alpha_2^2 - 2\alpha_2 + v_f^2(1-s_f^2) = 0 \qquad (2\text{-}3)$$

The overall optimization problem requires the minimization of the algebraic sum of both Δv's namely $\Delta v_1 + \Delta v_2$

$$\Delta v_1 + \Delta v_2 = \sqrt{\frac{1}{\alpha_1}} - v_1 + \sqrt{\frac{1}{\alpha_2}} - v_2 \qquad (2\text{-}4)$$

And with the use of (2-1), the performance index or payoff to maximize is

$$J = \frac{v_e\sqrt{1-s_e^2}}{\alpha_1} + \frac{v_f\sqrt{1-s_f^2}}{\alpha_2} \qquad (2\text{-}5)$$

with the side constraints (2-2) and (2-3) written in compact form

$$\omega_e(v_e, s_e) = 0 \quad ; \quad \omega_f(v_f, s_f) = 0 \qquad (2\text{-}6)$$

The transversality conditions at initial and final times are then

$$\lambda_{v_e} = -\frac{\partial J}{\partial v_e} - \nu_e \frac{\partial \omega_e}{\partial v_e}$$

$$\lambda_{s_e} = -\frac{\partial J}{\partial s_e} - \nu_e \frac{\partial \omega_e}{\partial s_e} \qquad (2\text{-}7)$$

$$\lambda_{v_f} = \frac{\partial J}{\partial v_f} + \nu_f \frac{\partial \omega_f}{\partial v_f}$$

$$\lambda_{s_f} = \frac{\partial J}{\partial s_f} + \nu_f \frac{\partial \omega_f}{\partial s_f}$$

where υ_e and υ_f are constant multipliers adjoint to the side constraints (2-6). The elimination of υ_e and υ_f in (2-7) leads to

$$\lambda_{v_e} = \frac{(\alpha_1^2 + s_e^2 - 1)}{v_e s_e} \lambda_{s_e} - \frac{\alpha_1}{\sqrt{1-s_e^2}} \qquad (2\text{-}8)$$

$$\lambda_{v_f} = \frac{(\alpha_2^2 + s_f^2 - 1)}{v_f s_f} \lambda_{s_f} + \frac{\alpha_2}{\sqrt{1-s_f^2}} \qquad (2\text{-}9)$$

If Δv_2 alone must be minimized, then only the side constraint $\omega_f(v_f,s_f)$ need to be taken into account since v_e,γ_e are then given and the corresponding transversality condition (2-9) considered only. λ_{h_f} is guessed and the corresponding values of λ_{v_f} and λ_{s_f} are obtained from (2-9) and (1-12) with $H_f=0$.

The system and Lagrange equations (1-9)-(1-11) and (1-13)-(1-15) are integrated backwards until $h_e=1$ at entry after a suitable guess of the exit s_f. λ_{h_f} is then adjusted until the entry v_e is matched. This procedure is repeated with a different guess of s_f until both entry conditions are matched namely v_e and s_e. The trajectory thus obtained represents the minimum ΔV_2 solution for given arbitrary entry state (v_e,s_e) and given target LEO. This particular two-point boundary value problem consists of a 2x2 search on (λ_{h_f}, s_f) in order to match the entry state (v_e,s_e).

For the more general case where $\Delta V_1 + \Delta V_2$ is minimized with prescribed α_1 and α_2, the two point boundary value problem is essentially identical to the one just described. λ_{h_f} and s_f are guessed and the backward integration carried out until (2-2) and (2-8) are satisfied. These iterations can also be carried out by forward integration; for example in the case of the minimization of $\Delta v_1 + \Delta v_2$, λ_{h_e} and s_e are guessed, v_e computed from (2-2), λ_{v_e} and λ_{s_e} computed from (2-8) and $H_e=0$ and the forward integration of both the system and multiplier sets carried out until $h_f=1$ and such that (2-3) and (2-9) are simultaneously satisfied. However it has been found that the backward integration is more stable because of the behavior of λ_v which exhibits a large gradient $d\lambda v/d\tau$ near exit making it very sensitive to the initial λ_{v_e} guess.

APPENDIX 3

The equations of motion assuming γ to be small are

$$\dot{V} = -\frac{D}{M} = \frac{\frac{1}{2}\rho V^2}{\beta} \qquad (3\text{-}1)$$

$$\dot{H} = V\gamma \qquad (3\text{-}2)$$

Assuming an exponential atmosphere, equations (1) and (2) can be rewritten, as follows:

$$\frac{dV}{V} = -\left(\frac{1}{2}\ \frac{\rho_o H_s}{\beta\gamma}\right) \exp\left(-\frac{H-H_o}{H_s}\right) \frac{dH}{H_s} \qquad (3\text{-}3)$$

Let us assume that over the exit interval that γ can be assumed to be an average constant, therefore

$$\ell n\left(\frac{V_e'}{V}\right) = k\left[\exp\left(\frac{H-H_E}{H_s}\right) - 1\right] \qquad (3\text{-}4)$$

An estimate of the exit speed can be made assuming a constant or reference β ref, as follows:

$$V_e' = V_{\exp}\left\{k\left[\exp\left(\frac{H-H_E}{H_s}\right) - 1\right]\right\} \qquad (3\text{-}5)$$

$$\text{where } k = \frac{\frac{1}{2}\rho_o V^2 H_s}{\beta_C \gamma V^2} = H_s \frac{\dot{V}}{V\dot{H}} \qquad (3\text{-}6)$$

V = Current computed airspeed
H = Current computed altitude
$\dot{H}$ = Current computed rate of climb
$\dot{V}$ = Current measured aerodynamic acceleration
β_C = Current commanded β

Conversely if the computed V_e' is greater than V_e desired, the new required or reference β can be computed as follows:

$$k_{Ref} = \frac{\ln\left({}^{V_e}/_V\right)}{\left[\exp\left(\frac{H-H_E}{H_s}\right) - 1\right]} \qquad (3\text{-}7)$$

and

$$\beta_{Ref} = \frac{q\ H_s}{k_{Ref}\ V\dot{H}} \qquad (3\text{-}8)$$

and q is inferred from current $\dot{V}$ and the previous command β or

$$q = \dot{V}\beta_C \qquad (3\text{-}9)$$

APPENDIX 4

Assuming a small γ, the equations of motion can be written as follows:

$$\ddot{H} = g\left(\frac{V^2}{V_s^2} - 1\right), \qquad (4\text{-}1)$$

Vertical acceleration

$$\dot{V} = -D = -\frac{1}{2}\rho\frac{V^2}{\beta} \quad (4\text{-}2)$$

Horizontal acceleration

where the ρ can be approximated by an exponential atmospheric model as follows:

$$\rho = \rho_o \exp\left[-(H-H_o)/H_s\right] \quad (4\text{-}3)$$

ρ_o = Reference ρ

H_o = Altitude at reference ρ

Taking the time derivative of drag, we get

$$\dot{D} = -\frac{D\dot{H}}{H_s} - \frac{2D^2}{V} \quad (4\text{-}4)$$

and the second derivative is

$$\ddot{D} = -\frac{\dot{D}\dot{H}}{H_s} - \frac{D\ddot{H}}{H_s} - \frac{4D\dot{D}}{V} - 2\frac{D^3}{V^2} \quad (4\text{-}5)$$

If we further assume that (D/V) *is approximately* zero for powers greater than one, we get

$$\ddot{D} = -\frac{\dot{D}\dot{H}}{H_s} - \frac{D\ddot{H}}{H_s} - \frac{4D\dot{D}}{V} \quad (4\text{-}6)$$

The difference equations in $\delta\dot{D}$, V, $\delta\dot{D}$, δD, $\delta\dot{H}$, and δV *are then*

$$\delta\ddot{D} = -\frac{D\delta\dot{H}}{H_s} - \frac{\dot{H}}{H_s}\delta\dot{D} - \frac{\ddot{H}\delta D}{H_s} - \frac{D}{H_s}\delta\ddot{H}$$

$$-4\frac{D}{V}\delta\dot{D} - 4\frac{D\dot{D}}{V^2}\delta V \quad (4\text{-}7)$$

From (4-6)

$$\delta\dot{D} = -\frac{\dot{H}}{H_s}\delta D - \frac{D\delta\dot{H}}{H_s} \quad (4\text{-}8)$$

From (4-4)

$$\delta\ddot{H} = \frac{2gV}{V_s^2}\delta V \quad (4\text{-}9)$$

From (4-1)

$$\delta V = \frac{V}{2D}\delta D + \frac{V}{2\beta}\delta\beta \quad (4\text{-}10)$$

From (4-2)

Assuming drag to be constant over a δV intervale, we get

$$\delta\ddot{D} + \left(\frac{\dot{H}}{H_s} + \frac{4D}{V}\right)\delta\dot{D} + \frac{\ddot{H}}{H_s}\delta D = \frac{D}{H_s}\delta\ddot{H} \quad (4\text{-}11)$$

$$\dot{H} = -\frac{2H_s}{V}D \quad (4\text{-}12)$$

The controller for β is a second order system as follows:

$$\delta\beta = C_1\delta D - C_2\delta\dot{H} \quad (4\text{-}13)$$

Substituting equations (8), (9), (10), (12) and (13) into equations (11), we get

$$\delta\ddot{D} + \left[\frac{2D}{V} + \frac{C_2}{\beta}\frac{V^2}{V_s^2}g\right]\delta\dot{D}$$

$$+\left[\frac{g}{H_s}\left(2\frac{V^2}{V_s^2} - 1\right) + \frac{C_1 gD}{H_s\beta}\frac{V^2}{V_s^2} + \frac{2C_2 g}{\beta}\frac{DV^2}{V_s^2}\right]\delta D = 0. \quad (4\text{-}14)$$

Using the standard form for a damped harmonic system, namely

$$\ddot{x} + 2\xi\omega\dot{x} + \omega^2 x = 0 \quad (4\text{-}15)$$

We get (D_{ref} = constant drag level)

$$C_2 = \frac{2(\xi\omega - D_{Ref}/V)}{g\left(V/V_s\right)^2}\beta_{Ref} \quad (4\text{-}16)$$

$$C_1 = \frac{H_s\left[\omega^2 - \frac{g}{H_s}\left(\frac{2V^2}{V_s^2} - 1\right)\right]}{D_{Ref}\quad g\left(\frac{V}{V_s}\right)^2}\beta_{Ref} - \frac{2H_s}{V}C_2 \quad (4\text{-}17)$$

where β_{Ref} is derived from the exit speed controller or estimator (Appendix 3).

The above gains can be computed every interval for commanding the β as follows:

$$\beta_C = \beta_{Ref} + C_1(D - D_{Ref}) - C_2(\dot{H} - \dot{H}_{Ref}) \quad (4\text{-}18)$$

$$\text{where } \dot{H}_{Ref} = -\frac{2H_s}{V}D_{Ref} \quad (4\text{-}19)$$